ELECTRONIC RESEARCH ARCHIVE
Volume **29**, Number **4**, September **2021**

doi:10.3934/era.2021012
pp. **2755–2770**

AN A POSTERIORI ERROR ESTIMATOR BASED ON LEAST-SQUARES FINITE ELEMENT SOLUTIONS FOR VISCOELASTIC FLUID FLOWS †

Hsueh-Chen Lee*

Center for General Education, Wenzao Ursuline University of Languages
900 Mintsu 1st Road Kaohsiung, Taiwan

Hyesuk Lee

School of Mathematical and Statistical Sciences, Clemson University
Clemson, SC 29634-0975, USA

Abstract. We present a posteriori error estimator strategies for the least-squares finite element method (LS) to approximate the exponential Phan-Thien-Tanner (PTT) viscoelastic fluid flows. The error estimator provides adaptive mass weights and mesh refinement criteria for improving LS solutions using lower-order basis functions and a small number of elements. We analyze an a priori error estimate for the first-order linearized LS system and show that the estimate is supported by numerical results. The LS approach is numerically tested for a convergence study and then applied to the flow past a slot channel. Numerical results verify that the proposed approach improves numerical solutions and resolves computational difficulties related to the presence of corner singularities and limitations arising from the exorbitant number of unknowns.

1. **Introduction.** The numerical simulation of viscoelastic fluid flows is challenging due to the strong coupling of governing equations and the large algebraic system with multiple dependent variables. Viscoelastic behavior of the fluid is often represented by a nonlinear constitutive model in the form of hyperbolic partial differential equations, which requires a stabilization technique for finite element approximations such as the streamline upwinding Petrov–Galerkin (SUPG) method and the discontinuous Galerkin method. In addition, finite element spaces for the velocity, pressure, and stress should satisfy the inf-sup condition if the standard mixed method is applied for numerical simulations. To overcome such difficulties, least-squares (LS) methods are frequently used to simulate viscoelastic flow problems [4, 6, 9, 14] because they provide the flexibility of choosing finite element spaces and no additional stabilization is needed. In this work we expand on the LS method [14] by considering a nonlinear a posteriori error estimator of residual type for the exponential Phan-Thien-Tanner (PTT) viscoelastic fluid.

2020 *Mathematics Subject Classification.* Primary: 65N30, 65N50, Secondary: 76A10.

Key words and phrases. Least-squares, viscoelastic fluid, adaptive mesh refinement, a posteriori error estimator, transverse slot.

The first author is supported by the Taiwan MOST grant 107-2115-M-160-001-MY2. The second author is grateful for the financial support provided in part by the US NSF grant DMS-1818842.

†The first author of this article would like to dedicate this article to her advisor Professor Tsu-Fen Chen (1956-2020) who was the main inspiration and guidance in her research in this area.

* Corresponding author: Hsueh-Chen Lee.

The PTT model is a popular viscoelastic model in polymeric fluid simulations [17, 16], where the extra-stress is written as a superposition of the polymeric and viscous stresses. The linear PTT model was proposed by Phan-Thien and Tanner in 1977, and Phan-Thien subsequently proposed the exponential PTT model in 1978. Ferrás et al. [7] reported that the exponential PTT model could behave more realistically in strong flows in which certain strain components grow exponentially in time. They also reported that the exponential model provided a better fit to experimental data.

A posteriori error estimators play an important role in measuring the accuracy of numerical solutions and can be used to guide adaptive refinements. They are also effective and reliable for error control [1, 4, 15]. Previous works on the Stokes equations and the linear PTT model [11, 14] show that an a posteriori error estimator serves as an indicator to adjust mass conservation weights on LS approaches to solve flows past a transverse slot. However, the numerical computations have been performed on uniform grids with more degrees of freedom. In [13], the results also show that grid effects of the LS method can not be reduced on some uniform refined grids, and geometric discontinuities cause corner singularities for flows in complex geometries.

On the basis of these studies, we consider an a posteriori error estimator for the exponential PTT model to adjust mass conservation weights and to develop mesh refinement criteria on the LS approach. Furthermore, we estimate the coercivity and continuity for the homogeneous LS functional, which involves the sum of the linearized equation residuals measured in the L^2-norm. The analysis of the linearized viscoelastic fluid using the LS method is extended from the proof presented in [14]. We propose an a posteriori error estimator of a residual type for the LS method as per considerations in the literature [8, 11, 15]. The convergence of the estimator is verified through convergence tests for a non-physical problem with a known solution, using properly adjusted weights for the LS functional. We extend the implementation to simulate the flow through a transverse slot using conforming piecewise polynomial elements for all unknowns. To capture the flow region and understand the flow feature, we modify the adaptive mesh algorithm in [10] using an a posteriori error estimator to refine grid points, and we compare numerical results by uniform and adaptive grids.

The organization of this paper is as follows. Section 2 presents the exponential PTT flow model and the LS functional for the Newton linearized system. In Section 3 the least squares problem is defined and the coercivity and continuity properties of the LS functional are proved. Section 4 presents an a priori error estimate for the LS approximations and introduces an a posteriori error estimator. Section 5 provides numerical results for numerical examples, and finally conclusions follow in Section 6.

2. Model problem.

The PTT model is one of widely used viscoelastic models in polymeric fluid simulations, where the extra-stress is written as a superposition of the polymeric stress $\boldsymbol{\sigma}$ and viscous stress $\boldsymbol{\tau}$ [2]. The viscous stress, which is associated with a solvent in some applications, is Newtonian, i.e., $\boldsymbol{\tau} = 2\eta_s \mathbf{D}$, where η_s is a constant viscosity and $\mathbf{D} = 0.5(\nabla \mathbf{u} + \nabla \mathbf{u}^T)$ is the standard strain rate tensor with the velocity $\mathbf{u}$. In the linearized form of the exponential PTT model, the polymer contribution to the stress obeys the following equation [2]

$$\boldsymbol{\sigma} e^{\frac{\varepsilon\lambda}{\eta_p}\mathrm{tr}(\boldsymbol{\sigma})} + \lambda(\mathbf{u}\cdot\nabla\boldsymbol{\sigma} - (\nabla\mathbf{u})^T\cdot\boldsymbol{\sigma} - \boldsymbol{\sigma}\cdot\nabla\mathbf{u}) = 2\eta_p\mathbf{D}. \tag{1}$$

In (1) λ is a relaxation time and η_p is the polymeric contribution to the viscosity, ϵ is the extensibility parameter in the range of $0 < \epsilon < 1$. The exponential term $e^{\frac{\epsilon\lambda}{\eta_p}\mathrm{tr}(\boldsymbol{\sigma})}$ can be expressed as

$$e^{\frac{\epsilon\lambda}{\eta_p}\mathrm{tr}(\boldsymbol{\sigma})} = 1 + \frac{\epsilon\lambda}{\eta_p}\mathrm{tr}(\boldsymbol{\sigma}) + \frac{1}{2}\left(\frac{\epsilon\lambda}{\eta_p}\right)^2 (\mathrm{tr}(\boldsymbol{\sigma}))^2 + O\left(\left(\frac{\epsilon\lambda}{\eta_p}\right)^3\right),$$

hence,

$$e^{\frac{\epsilon\lambda}{\eta_p}\mathrm{tr}(\boldsymbol{\sigma})} \approx 1 + \frac{\epsilon\lambda}{\eta_p}\mathrm{tr}(\boldsymbol{\sigma}) + \frac{a}{2}\left(\frac{\epsilon\lambda}{\eta_p}\right)^2 (\mathrm{tr}(\boldsymbol{\sigma}))^2. \tag{2}$$

The constitutive equation (1) with $a = 1$ is often referred to as the exponential PTT model and the equation is reduces to the linear PTT model when $a = 0$ [7].

Consider an incompressible exponential PTT viscoelastic fluid flow in $\Omega \subset R^2$ with the boundary Γ. Define the differential operators $\mathcal{G}_i$ for $i = 1, 2, 3, 4$ to describe the momentum equation, the mass conservation equation, the viscous constitutive equation, and the polymeric constitutive equation, respectively:

$$\mathcal{G}_1\boldsymbol{U} := Re(\mathbf{u}\cdot\nabla\mathbf{u}) - \nabla\cdot\boldsymbol{\sigma} - \nabla\cdot\boldsymbol{\tau} + \nabla p, \tag{3}$$

$$\mathcal{G}_2\boldsymbol{U} := \nabla\cdot\mathbf{u}, \tag{4}$$

$$\mathcal{G}_3\boldsymbol{U} := \boldsymbol{\tau} - 2\beta\mathbf{D}, \tag{5}$$

$$\mathcal{G}_4\boldsymbol{U} := We\left(\mathbf{u}\cdot\nabla\boldsymbol{\sigma} - (\nabla\mathbf{u})^T\cdot\boldsymbol{\sigma} - \boldsymbol{\sigma}\cdot(\nabla\mathbf{u})\right) + \boldsymbol{\sigma}\tilde{e}(\boldsymbol{\sigma}) - 2(1-\beta)\mathbf{D}, \tag{6}$$

where

$$\tilde{e}(\boldsymbol{\sigma}) := 1 + \frac{\epsilon We}{1-\beta}\mathrm{tr}(\boldsymbol{\sigma}) + \frac{a}{2}\left(\frac{\epsilon We}{1-\beta}\right)^2 (\mathrm{tr}(\boldsymbol{\sigma}))^2.$$

Collecting the constitutive equation (1) with the substitution (2) and by nondimensionalizaing, we have governing equations of the viscoelastic flow represented by the boundary value problem:

$$\mathcal{G}\boldsymbol{U} = \mathbf{F} \text{ in } \Omega, \tag{7}$$

$$\mathbf{u} = \mathbf{0} \text{ on } \Gamma, \tag{8}$$

where $\boldsymbol{U} := (\mathbf{u}, p, \boldsymbol{\tau}, \boldsymbol{\sigma})$, $\mathcal{G} := (\mathcal{G}_1, \mathcal{G}_2, \mathcal{G}_3, \mathcal{G}_4)$, $\mathbf{F} := (\mathbf{f}, 0, \mathbf{0}, \mathbf{0})$.

We assume that the scalar pressure p is fixed to p_0 at the point $\mathbf{x}_0$ on Γ, i.e., $p(\mathbf{x}_0) = p_0$, in order to ensure the uniqueness of pressure. $Re > 0$ is the Reynolds number given by $Re \equiv L_c U_c \rho/\eta_0$, in which $\eta_o = \eta_s + \eta_p$ is the zero-shear-rate viscosity, L_c and U_c are characteristic length and velocity, respectively. The parameter $\beta = \eta_s/\eta_o \in [0, 1]$ is the ratio of solvent viscosity to the total zero-shear-rate viscosity, which vanishes in the upper-convected Maxwell model. We is the Weissenberg number defined by $We \equiv \lambda U_c/L_c$ and $\mathbf{f}$ is the body force. In the case of $We = 0$, the model is reduced to the Newtonian model, the Navier-Stokes equations. The Oldroyd-B model is obtained if $\epsilon = 0$ in (2). Different types of the fluid models are summarized in Table 1.

To define the LS functional, we consider Newton linearization of the nonlinear equations (7)-(8) about known approximation $\mathbf{u}_n$, $\boldsymbol{\sigma}_n$ of the velocity and the polymeric stress tensor, respectively. The linearized system of the PTT model may now be written as

$$\mathcal{L}\boldsymbol{U} = \mathbf{F} \text{ in } \Omega, \tag{9}$$

$$\mathbf{u} = \mathbf{0} \text{ on } \Gamma, \tag{10}$$

TABLE 1. Viscoelastic fluid models for $(a,\ We,\ \beta,\ \epsilon)$

Constitutive equation	a	We	β	ϵ
Newtonian	0	0	β	0
Upper Convected Maxwell	0	We	0	0
Oldroyd-B	0	We	β	0
Linear PTT	0	We	β	ϵ
Exponential PTT	1	We	β	ϵ

where $\mathcal{L} := (\mathcal{L}_1, \mathcal{L}_2, \mathcal{L}_3, \mathcal{L}_4)$ and $\mathbf{F} := (\mathbf{f}_1, f_2, \mathbf{f}_3, \mathbf{f}_4)$, in which

$$\begin{aligned}
\mathcal{L}_1\boldsymbol{U} &:= Re(\mathbf{u}_n \cdot \nabla\mathbf{u} + \mathbf{u} \cdot \nabla\mathbf{u}_n) - \nabla \cdot \boldsymbol{\sigma} - \nabla \cdot \boldsymbol{\tau} + \nabla p, && (11)\\
\mathcal{L}_2\boldsymbol{U} &:= \nabla \cdot \mathbf{u}, && (12)\\
\mathcal{L}_3\boldsymbol{U} &:= \boldsymbol{\tau} - 2\beta\mathbf{D}, && (13)\\
\mathcal{L}_4\boldsymbol{U} &:= \mathcal{L}_{4,1}\boldsymbol{U} + \mathcal{L}_{4,2}\boldsymbol{U} + \mathcal{L}_{4,3}\boldsymbol{U} + \mathcal{L}_{4,4}\boldsymbol{U}, && (14)
\end{aligned}$$

and

$$\begin{aligned}
A(\nabla\mathbf{u}, \boldsymbol{\sigma}) &= (\nabla\mathbf{u})^T \boldsymbol{\sigma} + \boldsymbol{\sigma}(\nabla\mathbf{u}),\\
\mathcal{L}_{4,1}\boldsymbol{U} &:= \boldsymbol{\sigma} - 2(1-\beta)\mathbf{D},\\
\mathcal{L}_{4,2}\boldsymbol{U} &:= We\left(\mathbf{u} \cdot \nabla\boldsymbol{\sigma}_n + \mathbf{u}_n \cdot \nabla\boldsymbol{\sigma} - A(\nabla\mathbf{u}_n, \boldsymbol{\sigma}) - A(\nabla\mathbf{u}, \boldsymbol{\sigma}_n)\right),\\
\mathcal{L}_{4,3}\boldsymbol{U} &:= \left(\frac{\epsilon We}{1-\beta}\right)(\mathrm{tr}(\boldsymbol{\sigma_n})\boldsymbol{\sigma} + \mathrm{tr}(\boldsymbol{\sigma})\boldsymbol{\sigma}_n),\\
\mathcal{L}_{4,4}\boldsymbol{U} &:= \frac{a}{2}\left(\frac{\epsilon We}{1-\beta}\right)^2 \left[(\mathrm{tr}(\boldsymbol{\sigma}_n)\mathrm{tr}(\boldsymbol{\sigma}_n))\,\boldsymbol{\sigma} + 2\,(\mathrm{tr}(\boldsymbol{\sigma}_n)\mathrm{tr}(\boldsymbol{\sigma}))\,\boldsymbol{\sigma}_n\right],
\end{aligned}$$

and

$$\begin{aligned}
\mathbf{f}_1 &:= \mathbf{f} + Re(\mathbf{u}_n \cdot \nabla\mathbf{u}_n),\\
f_2 &:= 0\\
\mathbf{f}_3 &:= \mathbf{0}\\
\mathbf{f}_4 &:= We\left(\mathbf{u}_n \cdot \nabla\boldsymbol{\sigma}_n + A(\nabla\mathbf{u}_n, \boldsymbol{\sigma}_n)\right) + \left(\frac{\epsilon We}{1-\beta}\right)(\mathrm{tr}(\boldsymbol{\sigma}_n)\boldsymbol{\sigma}_n)\\
&\quad + \frac{a}{2}\left(\frac{\epsilon We}{1-\beta}\right)^2 (\mathrm{tr}(\boldsymbol{\sigma}_n)\mathrm{tr}(\boldsymbol{\sigma}_n))\,\boldsymbol{\sigma}_n.
\end{aligned}$$

The LS functional for (9)-(10) is then defined by

$$\mathcal{J}(\boldsymbol{U}; \mathbf{F}) = \sum_{j=1}^{4} \int_\Omega W_j(\mathcal{L}_j\boldsymbol{U} - \mathbf{f}_j)^2 d\Omega. \tag{15}$$

The weights of positive constants $W_1 = 1$, $W_2 = 10^m$ for $m = 1$ to 10, $W_3 = 1$, and $W_4 = (1 + We + \epsilon)^2$ are chosen on the basis of numerical tests under a wide range of parameters $(0 \le We \le 1,\ 1 \le Re \le 10,\ 0 \le \epsilon \le 1)$ in [14]. It is also shown in the work that the number of Newton iterative steps in the LS method is reduced by W_4. Note that the choice of weights is not dependent on Re because inertial effects in the viscoelastic fluid flows at low Re can be neglected.

Remark 1. Since the system of governing equations (7)-(8) is nonlinear, the linear functional (15) is minimized on each Newton iteration with $\mathbf{u}_n$, $\boldsymbol{\sigma}_n$ replaced by the solution of the previous Newton step.

3. **Least squares problem.** We consider the product space

$$\boldsymbol{\Phi} := \boldsymbol{V} \times Q \times \boldsymbol{\Sigma}_s \times \boldsymbol{\Sigma} := \mathbf{H}^1(\Omega)^2 \times L^2(\Omega) \times \mathbf{L}^2(\Omega)^2 \times \mathbf{L}^2(\Omega)^2.$$

The least-squares minimization problem for the solution of system (9)-(10) is to choose $\boldsymbol{U} \in \boldsymbol{\Phi}$ such that

$$\mathcal{J}(\boldsymbol{U};\mathbf{F}) \le \mathcal{J}(\boldsymbol{V};\mathbf{F}) \quad \forall \boldsymbol{V} \in \boldsymbol{\Phi}, \tag{16}$$

i.e., seek $\boldsymbol{U}$ such that $\mathcal{J}(\boldsymbol{U};\mathbf{F})$ is minimized over $\boldsymbol{\Phi}$.

To prove the coercivity and continuity of $\mathcal{J}$, we first define

$$\mathcal{J}_0 := \sum_{j=1}^{3} W_i \|\mathcal{L}_j \boldsymbol{U}\|_0^2 + W_4 \left\|\mathcal{L}_{4,1}\boldsymbol{U} + \mathcal{L}_{4,2}\boldsymbol{U} + \mathcal{L}_{4,3}\boldsymbol{U}\right\|_0^2. \tag{17}$$

Here, the norm $\|\cdot\|_0$ is associated with the inner products $(\cdot,\cdot)_{0,\,\Omega}$. The functional $\mathcal{J}_0$ can be used for the linear PTT, i.e., $\mathcal{J}_0 = \mathcal{J}(\boldsymbol{U};\mathbf{0})$ when $a = 0$ (or $\mathcal{L}_{4,4}\boldsymbol{U} = \mathbf{0}$ in (14)), and the a priori estimate for $\mathcal{J}_0$ is presented in [14]. Based on the result in [14] and (14), we establish an a priori estimate for the LS functional (15) in Theorem 3.1.

Theorem 3.1. *Suppose the known approximations $\mathbf{u}_n$, $\boldsymbol{\sigma}_n$ are uniformly bounded satisfying $\nabla \cdot \mathbf{u}_n = 0$, and*

$$M := \max\{\|\mathbf{u}_n\|_\infty,\ \|\nabla \mathbf{u}_n\|_\infty, \|\boldsymbol{\sigma}_n\|_\infty,\ \|\nabla \boldsymbol{\sigma}_n\|_\infty\} < \infty. \tag{18}$$

Then, for any $\boldsymbol{U} = (\mathbf{u}, p, \boldsymbol{\tau}, \boldsymbol{\sigma}) \in \boldsymbol{\Phi}$, there are positive constants, c_0 and c_1, which depend on Ω, β, We, α, and M, such that

$$c_0 \left(\|\mathbf{u}\|_1^2 + \|p\|_0^2 + \|\boldsymbol{\tau}\|_0^2 + \|\boldsymbol{\sigma}\|_0^2\right) \quad \le \quad \mathcal{J}(\boldsymbol{U};\mathbf{0})$$

and

$$\mathcal{J}(\boldsymbol{U};\mathbf{0}) \quad \le \quad c_1 \left(Re^2 \|\mathbf{u}\|_1^2 + \|p\|_1^2 + \|\boldsymbol{\tau}\|_1^2 + \|\boldsymbol{\sigma}\|_1^2\right)$$

if M is sufficiently small.

Proof. For a lower bound of $\mathcal{J}(\boldsymbol{U};\mathbf{0})$ we first consider the following estimate for $\mathcal{L}_{4,4}\boldsymbol{U}$.

$$\begin{aligned} \|\mathcal{L}_{4,4}\boldsymbol{U}\|_0 &= \frac{a}{2}\left(\frac{\epsilon We}{1-\beta}\right)^2 \left(\|\left(\mathrm{tr}(\boldsymbol{\sigma}_n)\mathrm{tr}(\boldsymbol{\sigma}_n)\right)\boldsymbol{\sigma}\|_0 + 2\|\left(\mathrm{tr}(\boldsymbol{\sigma}_n)\mathrm{tr}(\boldsymbol{\sigma})\right)\boldsymbol{\sigma}_n\|_0\right) \\ &\le 3a\left(\frac{\epsilon We}{1-\beta}\right)^2 \|\boldsymbol{\sigma}_n\|_0^2 \|\boldsymbol{\sigma}\|_0 \\ &\le 3a\left(\frac{\epsilon We}{1-\beta}\right)^2 M^2 \|\boldsymbol{\sigma}\|_0, \end{aligned} \tag{19}$$

and using the inequality $\|a+b\|_0^2 \ge (1/2)\|a\|_0^2 - \|b\|_0^2$, we have

$$\begin{aligned} \mathcal{J}(\boldsymbol{U};0) &\ge \frac{1}{2}\mathcal{J}_0 - W_4 \|\mathcal{L}_{4,4}\boldsymbol{U}\|_0^2 \\ &\ge \frac{1}{2}\mathcal{J}_0 - 3aW_4\left(\frac{\epsilon We}{1-\beta}\right)^2 M^2 \|\boldsymbol{\sigma}\|_0. \end{aligned} \tag{20}$$

It was proved in [14] that there exists a constant $\overline{C}_0 > 0$ satisfying

$$\mathcal{J}_0 \geq \overline{C}_0 \left(\|\mathbf{u}\|_1^2 + \|p\|_0^2 + \|\boldsymbol{\tau}\|_0^2 + \|\boldsymbol{\sigma}\|_0^2 \right)$$

if M is sufficiently small. Therefore, if $M^2 \leq \frac{\overline{C}_0}{12aW_4} \left(\frac{1-\beta}{\epsilon We} \right)^2$,

$$\begin{aligned} \mathcal{J}(\boldsymbol{U};\mathbf{0}) &\geq \frac{\overline{C}_0}{2} \left(\|\mathbf{u}\|_1^2 + \|p\|_0^2 + \|\boldsymbol{\tau}\|_0^2 \right) + \left(\frac{\overline{C}_0}{2} - \frac{\overline{C}_0}{4} \right) \|\boldsymbol{\sigma}\|_0^2 \\ &\geq c_0 \left(\|\mathbf{u}\|_1^2 + \|p\|_0^2 + \|\boldsymbol{\tau}\|_0^2 + \|\boldsymbol{\sigma}\|_0^2 \right), \end{aligned} \tag{21}$$

where $c_0 = \frac{\overline{C}_0}{4}$. Finally, the upper bound follows naturally from the triangle inequality. □

4. **A posteriori error estimator.** For the finite element approximation of (7)-(8), we assume that the domain Ω is a polygon and that $\mathcal{T}_h$ is a collection of finite elements such that $\Omega = \bigcup_{e \in \mathcal{T}_h} e$ with $h = \max\{\text{diam}(e) : e \in \mathcal{T}_h\}$. Assume that the triangulation $\mathcal{T}_h$ is regular and satisfies the assumption of inverse estimates [12]. The grid size is defined as $h = 2\sqrt{A}/\sqrt{N}$, where A is the area of the domain and N is the number of elements in $\mathcal{T}_h$. Let $P_r(e)$ denote the space of polynomials of degree less than or equal to r on element e. Define finite element spaces for the approximate of $(\mathbf{u}, p, \boldsymbol{\tau}, \boldsymbol{\sigma})$ by

$$\begin{aligned} \mathbf{V}^h &= \{\mathbf{v}^h \mid \mathbf{v}^h \in \mathbf{V} \cap (C^0(\Omega))^2,\ \mathbf{v}^h|_e \in P_{r+1}(e)^2\ \forall e \in \mathcal{T}_h\}, \\ Q^h &= \{q^h \mid q^h \in Q \cap C^0(\Omega),\ q^h|_e \in P_{r+1}(e)\ \forall e \in \mathcal{T}_h\}, \\ \boldsymbol{\Sigma}_s^h &= \{\zeta^h \mid \zeta^h \in \boldsymbol{\Sigma}_s \cap (C^0(\Omega))^{2\times 2},\ \zeta^h|_e \in P_{r+1}(e)^{2\times 2}\ \forall e \in \mathcal{T}_h\}, \\ \boldsymbol{\Sigma}^h &= \{\varsigma^h \mid \varsigma^h \in \boldsymbol{\Sigma} \cap (C^0(\Omega))^{2\times 2},\ \varsigma^h|_e \in P_{r+1}(e)^{2\times 2}\ \forall e \in \mathcal{T}_h\}. \end{aligned}$$

Let $\boldsymbol{\Phi}^h := \mathbf{V}^h \times Q^h \times \boldsymbol{\Sigma}_s^h \times \boldsymbol{\Sigma}^h$ be finite element subspaces of $\boldsymbol{\Phi}$ with the following approximation prosperities. Let $S^h = \{u \in C^0(\Omega) : u|_e \in P_{r+1}(e)\ \forall e \in \mathcal{T}_h\}$ admit the property

$$\inf_{u^h \in S^h} \left\| u - u^h \right\|_l \leq C h^m \|u\|_{m+l}\, \forall u \in H^{m+l}(\Omega), \tag{22}$$

for $m \leq r+1$ and $l = 0,\ 1$.

The discrete minimization problem for (16) is to choose $\boldsymbol{U}^h \in \boldsymbol{\Phi}^h$ such that

$$\mathcal{J}(\boldsymbol{U}^h;\mathbf{F}) = \inf_{\boldsymbol{V}^h \in \boldsymbol{\Phi}^h} \mathcal{J}(\boldsymbol{V}^h;\mathbf{F}), \tag{23}$$

where $\boldsymbol{U}^h = (\mathbf{u}^h, p^h, \boldsymbol{\tau}^h, \boldsymbol{\sigma}^h)$ and $\boldsymbol{V}^h = (\mathbf{v}^h, q^h, \boldsymbol{\zeta}^h, \boldsymbol{\varsigma}^h)$. Since $\boldsymbol{\Phi}^h$ is a finite element subspace of $\boldsymbol{\Phi}$. Then the solution is equivalently to find $\boldsymbol{U}^h \in \boldsymbol{\Phi}$ such that

$$\mathcal{B}(\boldsymbol{U}^h, \boldsymbol{V}^h) = \mathcal{F}(\boldsymbol{V}^h), \quad \forall \boldsymbol{V}^h \in \boldsymbol{\Phi}, \tag{24}$$

where

$$\mathcal{B}(\boldsymbol{U}^h, \boldsymbol{V}^h) := (\mathcal{L}\boldsymbol{U}^{\boldsymbol{h}}, \mathcal{L}\boldsymbol{V}^{\boldsymbol{h}}), \tag{25}$$

$$\mathcal{F}(\boldsymbol{V}^h) := (\mathbf{F}, \mathcal{L}\boldsymbol{V}^{\boldsymbol{h}}). \tag{26}$$

The following error estimate for the solution of (23) is obtained by the standard way, using the coercivity and continuity properties of the functional $\mathcal{J}$ in Theorem 3.1.

Theorem 4.1. *Consider approximating the solution to (9)-(10), where the known functions* $\mathbf{u}_n$, $\boldsymbol{\sigma}_n$ *are sufficiently close to* $\mathbf{u}$, $\boldsymbol{\sigma}$, *respectively, and satisfy the condition (18). Assume that* $\boldsymbol{U} \in \boldsymbol{\Phi} \cap \left(H^{m+1}(\Omega)\right)^2 \times H^{m+1}(\Omega) \times \left(H^{m+1}(\Omega)\right)^{2\times 2} \times \left(H^{m+1}(\Omega)\right)^{2\times 2}$ *is the solution to (16) and* $\boldsymbol{U}^h \in \boldsymbol{\Phi}^h$ *is the unique approximation solution to (23) for a small* M. *Then there is a positive constant* C *which is independent of* h *such that*

$$\|\mathbf{u}-\mathbf{u}^h\|_1 \le Ch^m\left(\|\boldsymbol{\tau}\|_{m+1}+\|\boldsymbol{\sigma}\|_{m+1}+\|p\|_{m+1}+Re\,\|\mathbf{u}\|_{m+1}\right), \tag{27}$$

$$\|p-p^h\|_0 \le Ch^m\left(\|\boldsymbol{\tau}\|_{m+1}+\|\boldsymbol{\sigma}\|_{m+1}+\|p\|_{m+1}+Re\,\|\mathbf{u}\|_{m+1}\right), \tag{28}$$

$$\|\boldsymbol{\tau}-\boldsymbol{\tau}^h\|_0 \le Ch^m\left(\|\boldsymbol{\tau}\|_{m+1}+\|\boldsymbol{\sigma}\|_{m+1}+\|p\|_{m+1}+Re\,\|\mathbf{u}\|_{m+1}\right), \tag{29}$$

$$\|\boldsymbol{\sigma}-\boldsymbol{\sigma}^h\|_0 \le Ch^m\left(\|\boldsymbol{\tau}\|_{m+1}+\|\boldsymbol{\sigma}\|_{m+1}+\|p\|_{m+1}+Re\,\|\mathbf{u}\|_{m+1}\right), \tag{30}$$

for $m \le r+1$.

Proof. By Theorem 3.1 and the approximation properties in (22), we have

$$\begin{aligned}\|\mathbf{u}-\mathbf{u}^h\|_1 &\le \left(\|\mathbf{u}-\mathbf{u}^{\mathrm{h}}\|_1^2+\|p-p^h\|_1^2+\|\boldsymbol{\tau}-\boldsymbol{\tau}^h\|_1^2+\|\boldsymbol{\sigma}-\boldsymbol{\sigma}^h\|_1^2\right)^{1/2}\\ &\le \inf_{V^h\in\Phi^h}\frac{c_1}{c_0}\left(Re^2\|\mathbf{u}-\mathbf{v}^{\mathrm{h}}\|_1^2+\|p-q^h\|_1^2+\|\boldsymbol{\tau}-\boldsymbol{\zeta}^h\|_1^2+\|\boldsymbol{\sigma}-\boldsymbol{\varsigma}^h\|_1^2\right)^{1/2}\\ &\le Ch^m\left(\|\boldsymbol{\tau}\|_{m+1}+\|\boldsymbol{\sigma}\|_{m+1}+\|p\|_{m+1}+Re\,\|\mathbf{u}\|_{m+1}\right).\end{aligned} \tag{31}$$

By the same approach, we can obtain the desired estimates for $\|p-p^h\|_0$, $\|\boldsymbol{\tau}-\boldsymbol{\tau}^h\|_0$, and $\|\boldsymbol{\sigma}-\boldsymbol{\sigma}^h\|_0$, respectively. □

Note that we obtain the error bounds $O(h)$ in the L^2-norm for $\boldsymbol{\tau}$, $\boldsymbol{\sigma}$, and p, $O(h)$ in the H^1-norm for $\mathbf{u}$ if continuous piecewise linear polynomials are used to approximate all unknowns functions. Hence, we have the optimal convergence rate of the velocity in the H^1-norm and suboptimal convergence rates of the stress and pressure in the L^2-norm.

For the residual of the first-order system (7)-(8), consider a nonlinear a posteriori error estimator of the following form:

$$g=\sum_{e\in\mathcal{T}_h} g_e, \quad \text{where} \quad g_e=\sum_{j=1}^{4}\|\mathcal{G}_j\boldsymbol{U}^h-\mathbf{F}\|_{0,e}^2 \tag{32}$$

and $\boldsymbol{U}^h=(\mathbf{u}^{\mathrm{h}},p^h,\boldsymbol{\tau}^h,\boldsymbol{\sigma}^h)$ is the finite element solution of (7)-(8) obtained by solving (24) iteratively by Newton's method. In numerical experiments the a posteriori error estimator g will be used to adjust the mass conservation weight W_2 in the LS functional (15). Also the convergence behavior of $g^{1/2}$ with respect to h will be numerically tested in the next section.

Theorems 3.1 and 4.1 require the small M condition, where M is a bound of the velocity and the stress. A viscoelastic fluid flow with a small M is a low-velocity flow, hence, we will consider low Re flows only for numerical tests.

5. Numerical experiments.

We consider two numerical examples. The first problem is chosen for convergence tests with the known exact solution in the unit square domain, and the second is a slot flow problem. All variables are approximated by P_1 polynomials, and the initial $\mathbf{u}_n$ and $\boldsymbol{\sigma}_n$ for Newton linearization are set to zero in all computations.

5.1. **Convergence tests.** Consider the flow in a planar channel on the domain $[0,1]\times[0,1]$ with the line of symmetry along $y=0$. Let $\mathbf{u}=(u,v)$ be specified along the boundary except on the axis of symmetry, and $\boldsymbol{\sigma}$ be specified on the inflow boundary where $\mathbf{u}\cdot\mathbf{n}<0$. The pressure $p=-1$ is set at the point $(1,\ 0)$, and v and $\boldsymbol{\sigma}_{xy}$ vanish on the axis of symmetry. The exact solution is chosen as $\mathbf{u}=(1-y^4,\ 0)^T$, $p=-x^2$, $\boldsymbol{\sigma}_{xx}=2We(1-\beta)\dot{\gamma}^2$, $\boldsymbol{\sigma}_{xy}=(1-\beta)\dot{\gamma}$, and $\boldsymbol{\sigma}_{yy}=0$, where $\boldsymbol{\sigma}$ represents the analytical solution for the linear PTT model of a steady-state shear flow [3]. The source terms in (7) are chosen appropriately for the exact solution. The modeling parameters are selected as $(a,\ We,\ \epsilon,\ Re,\ \beta)$=$(1,\ 0.2,\ 0.5,\ 1,\ 1/9)$.

First, in order to appropriately adjust the weight $W_2=10^m$ in (15), three uniform directional triangular meshes with 512, 2048, and 8192 elements are initially used. We iterate over m for $m=2,\ 3,\ \ldots,\ 10$, to investigate convergence of the functional $g^{1/2}$ in (32). Convergence of the iteration scheme with $W_2=10^m$ is declared when the relative norm of residual in the nonlinear functional between two consecutive iterations, $\delta g_m^{1/2}:=\|g_{m+1}^{1/2}-g_m^{1/2}\|/\|g_{m+1}^{1/2}\|$, is less than 10^{-4}. See Figure 1 for $\delta g_m^{1/2}$ by different m values. We observe that convergence is achieved at $m=6$, therefore, the mass conservation weight $W_2=10^6$ is used in the LS formulation for all computations in the first example.

Figure 2 shows the errors of LS solutions with $W_2=10^2$ and $W_2=10^6$, where for the case of $W_2=10^6$ we observe the consistent rates with the error estimate in Section 4; the rate for the velocity is optimal, $O(h)$ in the H^1-norm, and the rates for viscous and polymeric stresses, and pressure are suboptimal, $O(h)$ in the L^2-norm. Figure 2 shows that the convergent rates of LS solutions are higher for the larger $W_2(=10^6)$. These results also show the optimal convergence of $g^{1/2}$ at $O(h)$.

5.2. **Application: Flows past a transverse slot.** Consider the PTT flow past a slot in a channel for $-2.5\le x\le 2.5$ with the contraction occurring at $x=0$. See Figure 3. Let $\mathbf{u}=(u,v)$ and $\boldsymbol{\sigma}$ be specified on the inflow boundaries, and $\mathbf{u}=\mathbf{0}$ on the wall boundaries. Pressure p and v are set to zero at the outflow boundary. The forcing function $\mathbf{f}$ in (15) is set to $\mathbf{0}$. The system of model equations (7)-(8) is simulated with the parameter values $(a,\ We,\ \epsilon,\ Re,\ \beta)$=$(1,\ 0.1,\ 0.5,\ 1,\ 1/9)$.

5.2.1. *Mesh refinement criteria.* We consider the LS method (15) with the adaptively refined algorithms, which we name it the ALS method. This refinement technique is similar to the approach used for the Carreau model in [10]. For the mesh refinement strategy, we apply the grading function ϕ_e on elements e of a Mesh T given by $\phi_e=\|\nabla q\|_e$, where the scalar function q is calculated based on the a posteriori error estimator of LS solutions, i.e, $q=g_e^{1/2}$. Then, as in [10], the mesh redistribution function $f(\phi_e)$ is defined by

$$f(\phi_e)=|e|_{max}-(\phi_e-\phi_{e_{min}})\,\frac{\Delta|e|}{\Delta\phi_e},$$

where $|e|_{max}=\max\{|e|:\forall e\in T\}$, $\Delta|e|=|e|_{max}-|e|_{min}$ and $\Delta\phi_e=\phi_{e_{max}}-\phi_{e_{min}}$. If $e\in$ T satisfies $f(\phi_e)\le|e|$, then e is subdivided. We employ the a posteriori error estimator for mesh refinement criteria: $\Delta g_{(k)}^{1/2}/\Delta N_k=|g_{(k)}^{1/2}-g_{(k-1)}^{1/2}|/|N_k-N_{k-1}|$ where N_k represents the number of elements at the k-th refinement step and $g_{(k)}^{1/2}$ denotes the functional value by Mesh T_k. Figure 4 shows that a mesh convergence for N_k is confirmed when $\Delta g_{(k)}^{1/2}/\Delta N_k\ <2\times10^{-5}$, which yields convergence of Mesh

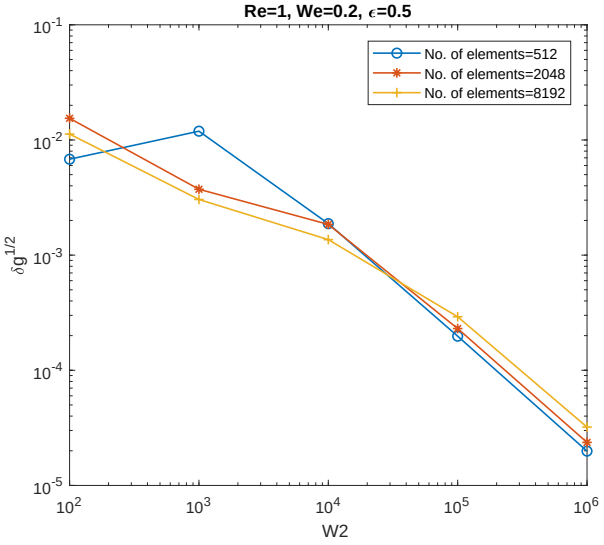

FIGURE 1. Reduction of the functional norm $\delta g_m^{1/2}$ on three meshes for various weights $W_2 = 10^m$ $(2 \le m \le 6)$.

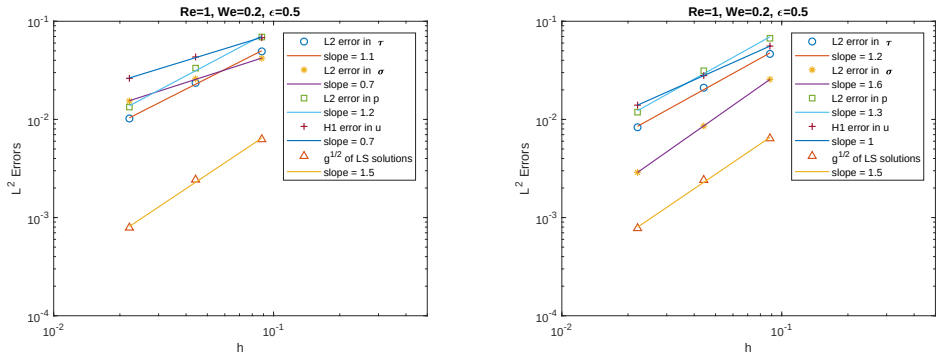

(a)$W_2 = 10^2$ (b)$W_2 = 10^6$

FIGURE 2. L^2 errors of $\boldsymbol{\tau}$, $\boldsymbol{\sigma}$, p, H^1 error in $\mathbf{u}$, and $g^{1/2}$ functional norm of the LS solutions for (a) $W_2 = 10^2$ and (b) $W_2 = 10^6$.

U at $k = 2$ with $N_2 = 25000$ and Mesh G at $k = 3$ with $N_3 = 12993$, respectively. Figure 5 shows Mesh G in the k-th refinement step for $k = 1$, 2, and 3 by the ALS method starting from the initial mesh T. The results show these adaptive meshes are highly refined near the corner. More details about meshes are given in Table 2.

5.2.2. *Weight adjustment criteria.* The optimal weight W_2 of the form $W_2 = 10^m$ is chosen in a similar manner to the first example; we iterate over m for $2 \le m \le 6$ for the functional $g_m^{1/2}$ in (32) on the uniformly refined Mesh T with 6144 elements. As shown in Figure 6, $\delta g_m^{1/2} = |g_{m+1}^{1/2} - g_m^{1/2}|/g_{m+1}^{1/2}$ is less than 10^{-4} at $m = 6$, therefore, $W_2 = 10^6$ is chosen as the optimal weight for the LS formulation. Figure 6 also shows $u(2.5,\ 0.5)$, the horizontal velocity u at $(2.5,\ 0.5)$, converges to 1.546

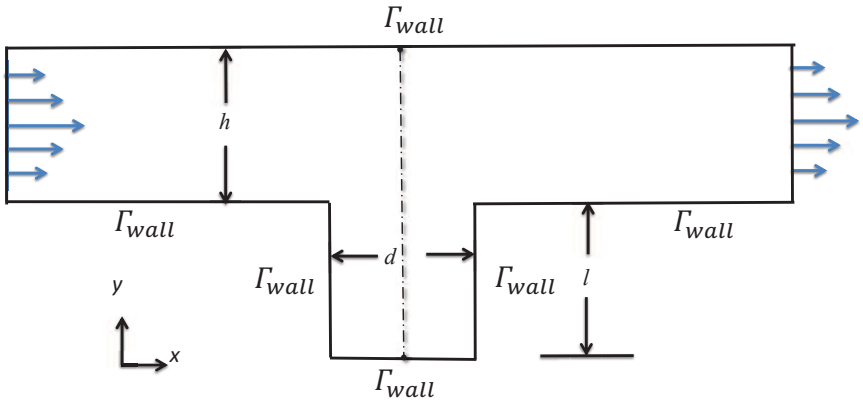

FIGURE 3. The slot channel with $d = h = l = 1$

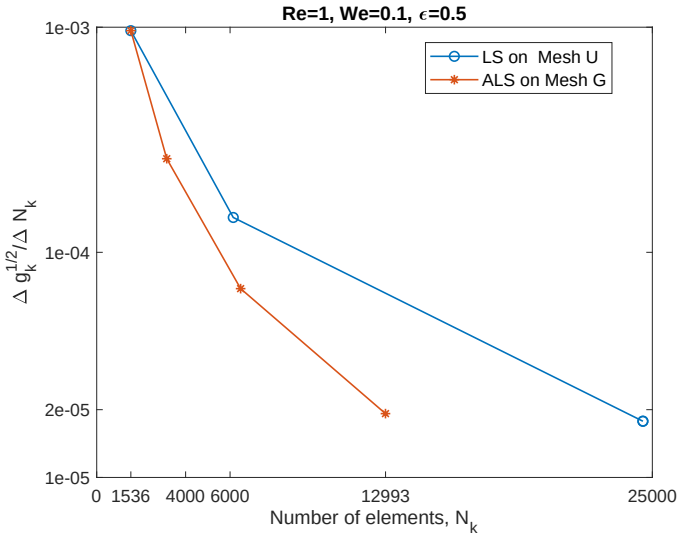

FIGURE 4. $\Delta g_{(k)}^{1/2}/\Delta N_k = |g_{(k)}^{1/2} - g_{(k-1)}^{1/2}|/|N_k - N_{k-1}|$ versus the number of elements N_k for k =1, 2, and 3, where $g_{(k)}^{1/2}$ denotes the functional value by N_k.

for $W_2 \geq 10^4$. Figure 7 shows streamlines of the LS solutions using $W_2 = 10^4$ and $W_2 = 10^6$, respectively. The figure shows that satisfactory solutions can be obtained by a sufficiently large weight, $W_2 = 10^6$, as shown in [11].

5.2.3. *Computation grids.* Grid independence results of $g^{1/2}$ and the convergence of $g^{1/2}$ by LS and ALS methods are presented in Figure 8(a) and (b), respectively. The figure shows that both LS and ALS methods yield the same convergent results

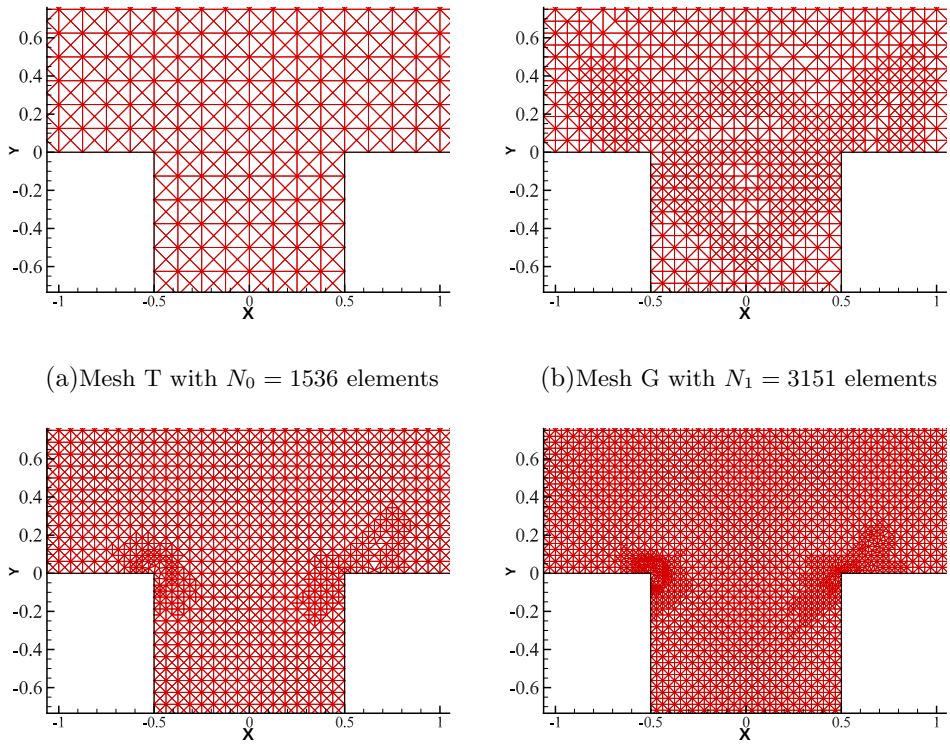

(a)Mesh T with $N_0 = 1536$ elements

(b)Mesh G with $N_1 = 3151$ elements

(c)Mesh G with $N_2 = 6475$ elements

(d)Mesh G with $N_3 = 12993$ elements

FIGURE 5. Mesh G with various number of elements N_k in refinement steps.

TABLE 2. Meshes considered for $(We,\ \epsilon,\ Re)$=(0.1, 0.5, 1).

Mesh	Type	Method	N_k [a]	S [b]	k [c]
Mesh S	Initial uniform grids	LS	348	4	–
Mesh T	Initial uniform grids	LS	1536	4	–
Mesh U	Uniform refined grids with Mesh T	LS	24576	5	2
Mesh G	Adaptive grids by $\boldsymbol{g}^{1/2}$ with Mesh T	ALS	12993	4	3
Mesh H	Adaptive grids by $\boldsymbol{g}^{1/2}$ with Mesh S	ALS	18320	4	5

[a] N_k represents the number of elements at the k refinement step.
[b] S is the number of Newton steps for convergence.
[c] k is the number of mesh refinements.

of $g^{1/2}$, $O(h)$. However, using the ALS method, the number of unknowns can be reduced from 111648 to 59551, therefore, the ALS method on Mesh G is more efficient than the LS method on Mesh U.

Furthermore, in Figure 9, we present contours of $g_e^{1/2}$ on uniform Meshes T and U by the LS method and adaptive Mesh G by the ALS method. Figures 9(b) and 9(c) show similar contours of $g_e^{1/2}$on Meshes U and G, respectively, and as shown in

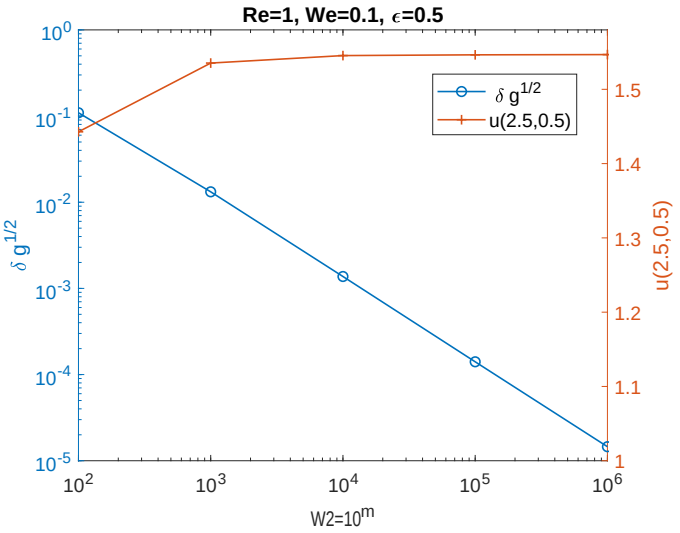

FIGURE 6. The LS solutions using $W_2 = 10^6$ on the uniformly refined Mesh U with 6144 elements. Reduction of functional norm $\delta g_m^{1/2}$ and $u(2.5, 0.5)$ for various weights $W_2 = 10^m$ $(2 \le m \le 6)$.

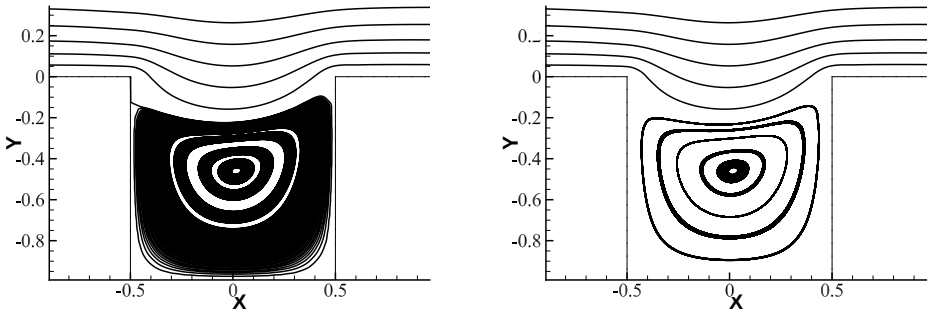

(a)$W_2 = 10^4$ (b)$W_2 = 10^6$

FIGURE 7. Streamlines of LS solutions on the refined Mesh U with 6144 elements using (a) $W_2 = 10^4$ and (b) $W_2 = 10^6$.

Figure 9(a), $g_e^{1/2}$ near the corner on Mesh T can be reduced using Meshes U and G. Thus, Meshes U and G reduce the residual error of the system generated by corner singularity. Using the ALS scheme, the number of elements can be reduced from 24576 (Mesh U) to 12993 (Mesh G), thus, the ALS method on Mesh G is more efficient than the LS method on Mesh U. Figure 10 presents contours of $g_e^{1/2}$ on the coarse uniform Mesh S and the adaptive Mesh H, respectively. The results indicate that $g_e^{1/2}$ on Mesh S can be reduced by Mesh H. Note that the contours of $g_e^{1/2}$ on Meshes G and H in Figures 9(c) and 10, respectively, are almost in agreement. For the initial Mesh T, the number of elements and the refinement steps can be reduced from 18320 (Mesh H) to 12993 (Mesh G) and from 5 (Mesh H) to 3 (Mesh G),

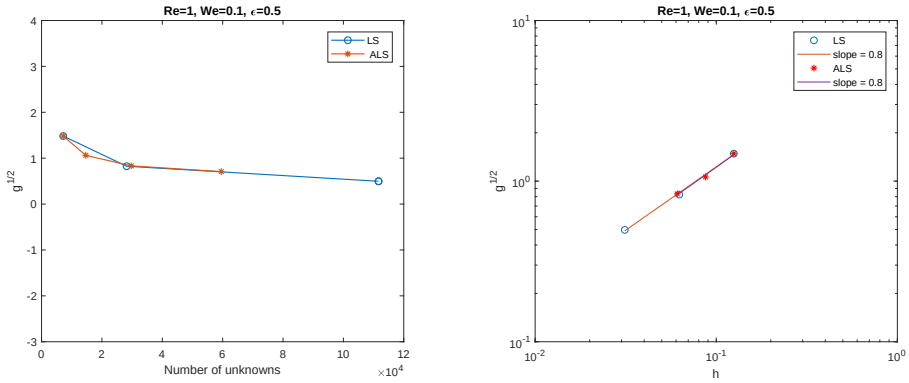

(a) (b)

FIGURE 8. LS solutions at $Re = 1$, $We = 0.1$, and $\epsilon = 0.5$ using $W_2 = 10^6$. (a) Grid independence results for $g^{1/2}$. (b) Convergence of $g^{1/2}$ by the LS and ALS methods.

respectively. Thus, Mesh T as the initial Mesh for the ALS method outperforms the initial Mesh S.

Finally, we compare streamlines of the ALS solutions for the exponential PTT ($a = 1$), linear PTT ($a = 0$), and the Oldroyd-B ($\epsilon = 0$) models at $We = 1$. Figure 11 shows that vortices for $We = 1$ fluids. The vortices of the fluids move toward the reentrant corners and are consistent with those obtained on uniform grids in [14]. The result shows that the shear-thinning behavior of the exponential PTT flow seems to be more obvious than the linear PTT or Oldroyd-B flows.

6. **Conclusion.** We considered a nonlinear a posteriori error estimator based on a first-order LS method for the exponential PTT viscoelastic model of strong flows. The LS method was developed by assigning proper weights to the terms of the LS functional, in which the mass conservation weights are obtained by the a posteriori error estimator. We also proposed an adaptive LS (ALS) for the exponential PTT model, where the a posteriori error estimator of the LS solution is used for adaptive mesh refinements. The proposed approach resolves some difficulties related to the presence of corner singularities in this second example. In addition, the ALS approach with adaptive mesh refinements improves computational efficiency.

REFERENCES

[1] J. H. Adler, T. A. Manteuffel, S. F. McCormick, J. W. Nolting, J. W. Ruge and L. Tang, Efficiency based adaptive local refinement for first-order system least-squares formulations, *SIAM J. Sci. Comput.*, **33** (2011), 1–24.

[2] M. A. Alves, P. J. Oliveira and F. T. Pinho, Benchmark solutions for the flow of Oldroyd-B and PTT fluids in planar contractions, *J. Non-Newtonian Fluid Mech.*, **110** (2003), 45–75.

[3] R. B. Bird, R. C. Armstrong and O. Hassager, *Fluid Mechanics, Dynamics of Polymeric Liquids, Volume 1: Fluid Mechanics*, 2nd ed. New York, John Wiley and Sons, 1987.

[4] Z. Cai and C. R. Westphal, An adaptive mixed least-squares finite element method for viscoelastic fluids of Oldroyd type, *J. Non-Newtonian Fluid Mech.*, **159** (2009), 72–80.

[5] T. F. Chen, C. L. Cox, H. C. Lee and K. L. Tung, Least-squares finite element methods for generalized Newtonian and viscoelastic flows, *Appl. Numer. Math.*, **60** (2010), 1024–1040.

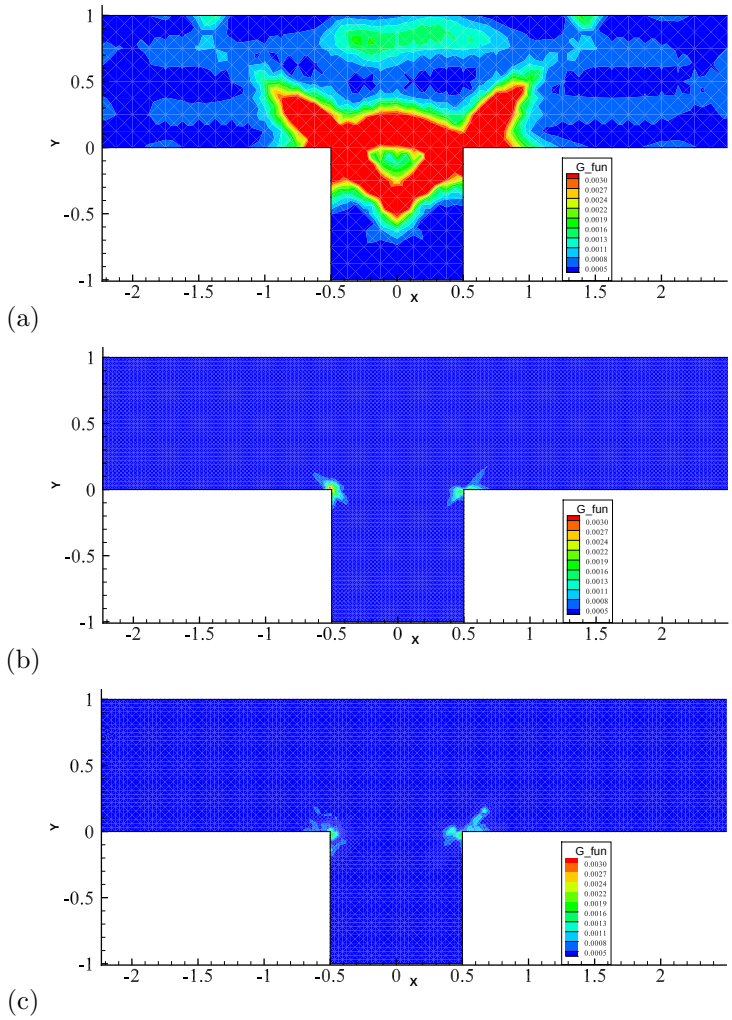

FIGURE 9. Plots of $g_e^{1/2}$ on (a) the initial Mesh T with 1536 elements, (b) the uniformly refined Mesh U with 24576 elements, and (c) the adaptive Mesh G with 12993 elements.

[6] T. F. Chen, H. Lee and C. C. Liu, Numerical approximation of the Oldroyd-B model by the weighted least-squares/discontinuous Galerkin method, *Numer. Methods Partial Differ. Equations*, **29** (2013), 531–548.

[7] L. L. Ferrás, M. L. Morgado, M. Rebeloc, Gareth H. McKinley and A. M. Afonso, A generalised Phan-Thien-Tanner model, *J. Non-Newtonian Fluid Mech.*, **269** (2019), 88–89.

[8] J. Ku and E. J. Park, A posteriori error estimators for the first-order least-squares finite element method, *J. Comput. Appl. Math.*, **235** (2010), 293–300.

[9] H. C. Lee, A nonlinear weighted least-squares finite element method for the Oldroyd-B viscoelastic flow, *Appl. Math. Comput.*, **219** (2012), 421–434.

[10] H. C. Lee, An adaptively refined least-squares finite element method for generalized Newtonian fluid flows using the Carreau model, *SIAM J. Sci. Comput.*,**36** (2014), 193–218.

[11] H. C. Lee, Adaptive weights for mass conservation in a least-squares finite element method, *Int. J. Comput. Math.*, **95** (2018), 20–35.

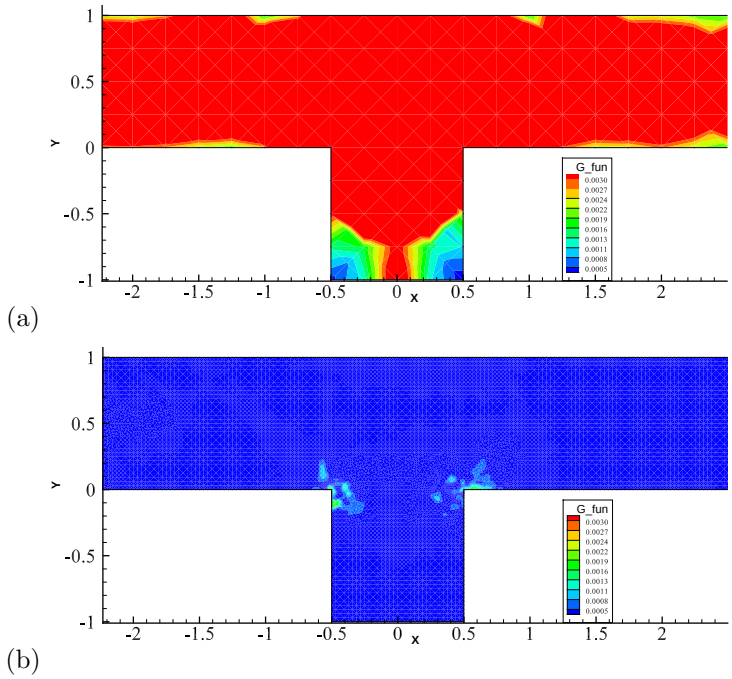

FIGURE 10. Plots of $g_e^{1/2}$ on (a) the initial Mesh S with 384 elements and (b) the adaptive Mesh H with 18320 elements at the 5-th refinement step.

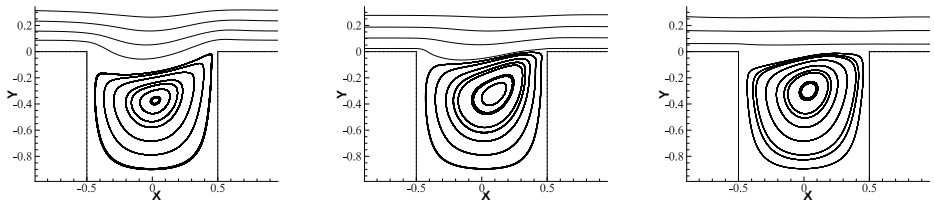

(a) Exponential PTT at $We = 1$ (b) Linear PTT at $We = 1$ (c) Oldroyd-B at $We = 1$

FIGURE 11. Streamlines of the flow over a slot by the ALS method for (a) the exponential PTT ($a = 1$), (b) the linear PTT ($a = 0$), and (c) the Oldroyd-B ($\epsilon = 0$) models at $We = 1$.

[12] H. C. Lee and T. F. Chen, A nonlinear weighted least-squares finite element method for the Stokes equations, *Comput. Math. Appl.*, **59** (2010), 215–224.
[13] H. C. Lee and T. F. Chen, Adaptive least-squares finite element approximations to Stokes equations, *J. Comput. Appl. Math.*, **280** (2015), 396–412.
[14] H. C. Lee and H. Lee, Numerical simulations of viscoelastic fluid flows past a transverse slot using least-squares finite element methods, *J. Sci. Comput.*, **79** (2019), 369–388.
[15] J. L. Liu, Exact a posteriori error analysis of the least squares finite element method, *Appl. Math. Comput.*, **116** (2000), 297–305.
[16] N. P. Thien, A nonlinear network viscoelstic model, *J. Rheol.*, **22** (1978), 259–283.

[17] N. P. Thien and R. I. Tanner, A new constitutive equation derived from network theory, *Journal of Non-Newtonian Fluid Mechanics*, **2** (1977), 353–365.

Received July 2020; revised December 2020.

E-mail address: 87013@mail.wzu.edu.tw
E-mail address: hklee@clemson.edu